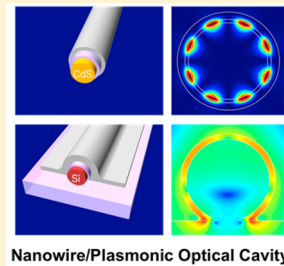


Tailoring the Spectroscopic Properties of Semiconductor Nanowires via Surface-Plasmon-Based Optical Engineering

Carlos O. Asperti and Ritesh Agarwal*

Department of Materials Science and Engineering, University of Pennsylvania, Philadelphia, Pennsylvania 19104, United States

ABSTRACT: Semiconductor nanowires, due to their unique electronic, optical, and chemical properties, are firmly placed at the forefront of nanotechnology research. The rich physics of semiconductor nanowire optics arises due to the enhanced light–matter interactions at the nanoscale and coupling of optical modes to electronic resonances. Furthermore, confinement of light can be taken to new extremes via coupling to the surface plasmon modes of metal nanostructures integrated with nanowires, leading to interesting physical phenomena. This Perspective will examine how the optical properties of semiconductor nanowires can be altered via their integration with highly confined plasmonic nanocavities that have resulted in properties such as orders of magnitude faster and more efficient light emission and lasing. The use of plasmonic nanocavities for tailored optical absorption will also be discussed in order to understand and engineer fundamental optical properties of these hybrid systems along with their potential for novel applications, which may not be possible with purely dielectric cavities.



When light is incident on a material, it will interact with that material by moving the bound and free charges, which gives rise to all of the optical phenomena.¹ Yet some of the most interesting effects arise when light interacts with active media, that is, materials that have electronic resonances, which themselves are optical emitters. Edward Purcell was the first to recognize that the rate of light emission from any dipole source is a function of the surroundings of the emitter and can be computed via

$$\gamma = \frac{3Q}{4\pi^2} \left(\frac{\lambda^3}{V_m} \right) \gamma_0$$

where γ_0 is the spontaneous emission rate in free space, λ is the wavelength of the emitted radiation in the host medium, Q is the quality factor of the electromagnetic mode coupling to the optical emitter, and V_m is the mode volume of the same.² The quality factor is a measure of the ability of the surroundings to store electromagnetic energy, analogous to how a capacitor stores electrical energy. It is also a measure of how long light is confined in the host system before radiating into the vacuum. In the denominator, the effective mode volume, which may be expressed as

$$V_m = \frac{\int \epsilon(r) E^2(r) d^3r}{(\epsilon(r) E^2(r))_{\max}}$$

represents the level of confinement of the electromagnetic mode (it has units of volume and is often quoted with respect to λ^3). The enhancement in the spontaneous emission rate (γ/γ_0) is known as the Purcell factor, according to which, in order to achieve high light emission rates, optical emitters should be placed in regions where the optical modes are long-lived (high Q) and highly confined (low V_m), two quantities that are typically anticorrelated. Implicit in the above expression

is that the optical modes of the surroundings of the emitter (i.e., the optical cavity) be spectrally matched to the emission frequency of the optical emitter. In fact, in order to compute an accurate Purcell factor, additional corrections for spectral and spatial matching between the emitter and electromagnetic modes of the cavity must be taken into account.³ The physical origin of the Purcell effect lies in Fermi's golden rule, where the spontaneous emission rate of an optical emitter is computed via

$$\gamma = \frac{2\pi}{\hbar} |\langle f | \vec{d} \cdot \vec{E}(\vec{r}) | i \rangle|^2 \rho(\hbar\omega)$$

and where $\langle f | \vec{d} \cdot \vec{E}(\vec{r}) | i \rangle$ is the transition dipole matrix element for the transition between the initial state i and final state f and $\rho(\hbar\omega)$ is the photon density of states. The ratio Q/V_m is related to the photon density of states in the quantum mechanical picture and is made explicit in the derivation of the Purcell effect directly from Fermi's golden rule (see the recent review by Maier et al.⁴).

Though initially developed for radio frequency operation, the Purcell effect is a general principle that can be applied in the visible regime. The wavelength of radio waves is on the order of a meter, with the corresponding antenna sizes in the centimeter to millimeter range. For optical waves (<1 μm), the resonant antenna size would fall into the nanoscale range, requiring significant effort in their design and fabrication. However, impressive advances in nanofabrication have allowed us to engineer optical cavities with nanoscale dimensions, thus tuning their electromagnetic resonances to the UV–visible–near IR region of the electromagnetic spectrum; a beneficial feature noting band gaps and light emission from many important elemental

Received: August 28, 2014

Accepted: October 10, 2014

Published: October 10, 2014

If we are mostly interested in enhancing spontaneous emission, that is, for applications in lighting or light sources for spectroscopy on a chip, then a better design could be to optimize Q/V_m (or the photon density of states) not through high Q and low V_m but rather through low Q and extremely low V_m values, that is, below the diffraction limit.

and compound semiconductors (Si, Ge, GaN, InP, GaAs, etc.) typically falls in this spectral range.⁵ In general, the dimensions of dielectric optical cavities are limited by the diffraction limit, that is, light cannot be confined to dimensions much smaller than $\lambda/2n$ in the host medium with refractive index n , thereby placing a constraint on the effective mode volume. In response, research has focused on optical cavities that optimize the quality factor, Q . Whispering gallery mode (WGM) resonators operating in the visible range have achieved Purcell factors > 100 with a quality factor of 12 000.⁶ Furthermore, Q factors as high as 10^8 have been achieved at IR wavelengths in WGM structures.⁷ Benefits of high Q cavities such as long photon lifetimes⁸ include enhanced light–matter interactions leading to interesting phenomena related to cavity quantum electrodynamics applications^{8,9} and highly sensitive biological detectors.¹⁰ On the other hand, such optical cavities generally require a large footprint as optical losses increase with light confinement, hindering their use in nanoscale devices. This method of optimizing Q/V_m introduces another disadvantage; a higher-quality factor equates to a narrower mode in frequency space (<1 meV in the case of the WGM system described above), thereby limiting the operational bandwidth of the hybrid optical cavity-active material device. Thus, if we are mostly interested in enhancing spontaneous emission, that is, for applications in lighting or light sources for spectroscopy on a chip, then a better design could be to optimize Q/V_m (or the photon density of states) not through high Q and low V_m but rather through low Q and extremely low V_m values, that is, below the diffraction limit.

Metals excel at confining light into deep-subwavelength dimensions in the optical regime. When light is incident on the surface of a metal in the spectral region where the metal has negative values of permittivity, it can couple strongly with the surface electrons to form surface plasmon polaritons (SPPs).¹¹ The surface electrons serve to “anchor” the light to the surface of the metal, resulting in an electromagnetic mode that may only propagate on the surface of the metal. In a similar fashion, localized surface plasmons (LSPs) are nonpropagating modes, which may be excited in deep-subwavelength (nano)structures where the light–matter interaction may be treated quasistatically.¹² Physically speaking, the key difference between SPPs and LSPs is that LSPs are not bound to the same dispersion relation as SPPs, which facilitates their excitation from the far-field.¹² Furthermore, the LSP resonances of deep-subwavelength metal nanostructures are known to be a sensitive function of both size and geometry.^{12,13}

Metals with high free electron densities, such as Ag and Au, possess surface plasmon resonances in the visible regime. Au nanostructures, for example, interact with light with wavelengths on the order of a micrometer and confine it to dimensions of a few nanometers, ~ 100 times smaller, far below the diffraction limit.^{14–16} In other words, these metal nanostructures are simply antennas that operate at optical frequencies. Though metal nanostructures can enhance light emission in materials via the Purcell effect (discussed below) and the associated increase in photon density of states with highly confined light, yet another way to examine the potential of optical nanoantennas to enhance light emission is to examine the effect of length scales. From the perspective of classical antenna design, the power emitted by a time-harmonic current element of length l is directly proportional to $(l/\lambda)^2$, where λ is the wavelength of the emitted light. The optical dipoles in materials, which are the sources of light emission, represent the small radiating current elements given their oscillations in nanoscale (or even smaller) dimensions. On the other hand, the light that they emit (e.g., in the visible range) has wavelengths that are several orders of magnitude larger. This length-scale mismatch leads to, for example, the low absorption cross sections and low emission quantum efficiencies of single molecules.¹⁷ Optical antennas mitigate this length-scale mismatch by confining light to dimensions more amenable to the length scales of an electron confined in a molecule and have led to significant enhancements in fluorescence intensity ($>10^3$)¹⁶ and Purcell enhancements up to ~ 30 times^{16,18} for single molecules. We refer the reader to several excellent reviews for more discussion on relating radio frequency antenna theory to metallic nanostructures,¹⁷ optical antenna action (i.e., redirection of light emission and polarization),^{4,17} optical-antenna-enhanced quantum yield,^{4,19} and applications thereof.^{4,17,19,20}

Surface-plasmon-based devices, where the exciting source is light from the far field and where the only spectrally matched material resonance is that of the plasmonically active medium, have enabled applications such as single-molecule detection,^{21,22} targeted cancer therapy,²³ more efficient solar cells,²⁴ and even optical cloaking.²⁵ The physics of these devices is certainly interesting in its own right, but yet, another level of complexity arises when surface plasmons are interfaced with active materials, that is, materials with electronic resonances that are spectrally matched to the surface plasmon resonance. Tailoring of the light emission properties of active materials is one such application that has received significant attention in recent years and is largely based on the interaction between optical antennas and active media.^{16,18,26–29} It should be noted that the term “active plasmonics” has also been employed regarding systems where the propagation of SPPs is controlled by changing the dielectric environment, that is, via passive means.³⁰ In this Perspective, “active” refers exclusively to the active material with electronic resonances that interact with the plasmonically active metal.

The tailoring of spontaneous emission lifetimes (Purcell enhancement) of organic molecules via coupling to surface plasmons has been studied since the 1960s,³¹ with early experiments demonstrating both fluorescence enhancement^{32,33} and quenching^{34,35} of the spontaneous emission intensity. Indeed, it was recently shown, both experimentally and theoretically, that surface-plasmon-enhanced spontaneous emission can transition from a region of emission enhancement to quenching with decreasing separation from a metal surface.³⁶ This is due to the interplay between increasing excitation rate,

which increases monotonically with decreasing separation from the metal, and the quantum yield, which initially increases but eventually peaks as nonradiative pathways are augmented with proximity to the metal surface. Metallic nanostructures have been interfaced with both organic and inorganic optical emitters, leading to Purcell factors of up to ~ 100 , and where the Purcell enhancements are based on interfacing with both LSP modes^{16,18,36–43} and SPP modes.^{28,44–49} The highest Purcell enhancements of $\sim 10^3$ were recently demonstrated in semiconductor nanowires (NWs) integrated with plasmonic nanocavities (discussed later).^{26,27} These systems constitute more efficient light emitters, where optoelectronic devices based on their emission may be modulated at frequencies up to 1000 times that of their bulk counterparts, yet an even more technologically relevant application is the development of truly nanoscopic laser sources. By coupling surface plasmon modes with a gain medium, the surface plasmons themselves may be amplified by making multiple passes through the medium embedded in metal nanostructures, resulting in surface plasmon amplification by stimulated emission of radiation, also known as SPASER action.⁵⁰ A more general term, “plasmonic laser”, which employs surface plasmons to enhance lasing (i.e., propagating SPP- and LSP-based), has also been used in recent literature.^{29,51} Optically pumped plasmon lasers have been synthesized via both LSPs and SPPs such as in a Au nanoparticle functionalized with an organic dye⁴¹ and a CdS nanocrystal interfaced with a Ag film.^{29,49} All cases led to lasing from deep-subwavelength regions and enhanced spontaneous emission. As will be discussed later, these enhanced properties (both Purcell enhancement and surface-plasmon-based lasing) can be taken to even higher extremes by interfacing surface plasmons with 1-D active structures, that is, semiconductor NWs. Furthermore, we would like to note that strong light–matter coupling between surface plasmons and excitons (electron–hole pairs) in active media has been predicted⁵² and observed,^{53–56} where the surface plasmon and exciton form yet another strongly coupled quasi-particle, that is, polaritons. Unlike Purcell enhancement, which is a “weak”-coupling phenomenon, strong light–matter interaction is possible when the dephasing time scale of both the surface plasmon and exciton is longer than the time that it takes for energy to be transferred between the exciton and plasmon (generally referred to as Rabi oscillations), resulting in the formation of polaritons. We will omit discussion on strong light–matter coupling with surface plasmons as it is outside of the scope of this Perspective but refer the interested reader to a brief review on the subject and references therein.⁵⁷

The physics of these devices is certainly interesting in its own right, but yet, another level of complexity arises when surface plasmons are interfaced with active materials, that is, materials with electronic resonances that are spectrally matched to the surface plasmon resonance.

Most recently, surface-plasmon-enhanced light emission was extended to semiconductor NWs, which have been the subject of intense research activity⁵⁸ due in part to their unique

electronic⁵⁹ and optical⁶⁰ properties and also to their ease of fabrication in myriad compositions.⁶¹ The rich physics of semiconductor NW optics stems from their ability to serve as both optical cavities and sources of light. Semiconductors are generally high refractive index materials such that semiconductor NWs can effectively trap light if their dimensions are larger than the effective wavelength in the material. In other words, NWs serve as optical cavities but with dimensions still on the order of the diffraction limit. NW optical cavity resonances are comprised of standing waves formed along the NW long axis, in other words, with the k vector parallel to the long axis (waveguided modes) and those that propagate in the cross section of the NW, with the k vector perpendicular to the long axis (WGMs^{62,63}). The waveguided modes of dielectric cylindrical waveguides are readily described by solving Maxwell's equations⁶⁴ but with the potential for significant guiding of light outside of the NW due to the nanoscale dimensions that are on the order of the wavelength of the light.⁶⁵ These waveguided modes, coupled with the electronic properties of semiconductor NWs, have produced highly sensitive photodetectors^{66,67} and nanoscale lasers, which are both optically and electrically pumped.^{68,69} The WGMs have been used to enhance light absorption in semiconductor NWs with direct applications as improved photodetectors⁶³ and which couple the enhanced electronic properties of semiconductor NW solar cells⁷⁰ with their light trapping ability for even higher efficiency.⁷¹ As discussed above, all-dielectric WGM resonators typically require very large footprints in order to optimize the ratio Q/V_m ^{6,7} as the quality factor is directly proportional to the azimuthal order of the WGM mode^{72,73} and the mode volume is constrained by the diffraction limit.

Furthermore, due to the particularly high oscillator strengths found in many compound semiconductor materials, excitons in semiconductor NWs may couple strongly to light to form a polariton, that is, exciton–polariton. Thus, NWs serve as both optical cavities and nanoscopic sources of strongly coupled light. For an in-depth overview of light–matter interaction in semiconductor NWs, we refer the reader to recent reviews on the subject.^{74,75} Our recently developed understanding of the spectroscopic properties of semiconductor NWs, which again stems from the electromagnetics of subwavelength NW optical cavities and their light-emitting processes, has led to novel physical phenomena such as tunable light–matter coupling⁷⁶ and, from an applications perspective, all-optical logic gates based on polariton–polariton scattering.⁷⁷

With this understanding of semiconductor NW optics, the next step is to tune the spectroscopic properties of NWs with nanophotonics, that is, by interfacing NWs with plasmonic nanocavities, further confining light to dimensions far below the diffraction limit. Certainly, many of the principles of Q/V_m optimization outlined above may be applied to semiconductor NWs, but yet another level of complexity is attained due to the fact that these NWs also act as optical cavities (discussed above). Thus, as we will observe in the following discussion, tuning of the spectroscopic properties of semiconductor NWs will involve the interplay between NW cavity modes and the surface plasmon modes of plasmonic nanocavities, which will result in the engineering not only of their light emission properties but also of the absorption/scattering properties of the plasmonically coupled NWs.

Figure 1a–c demonstrates three different paradigms for the integration of semiconductor NWs with surface plasmons based on recent works by Oulton et al.²⁹ and Cho et al.^{26,27}

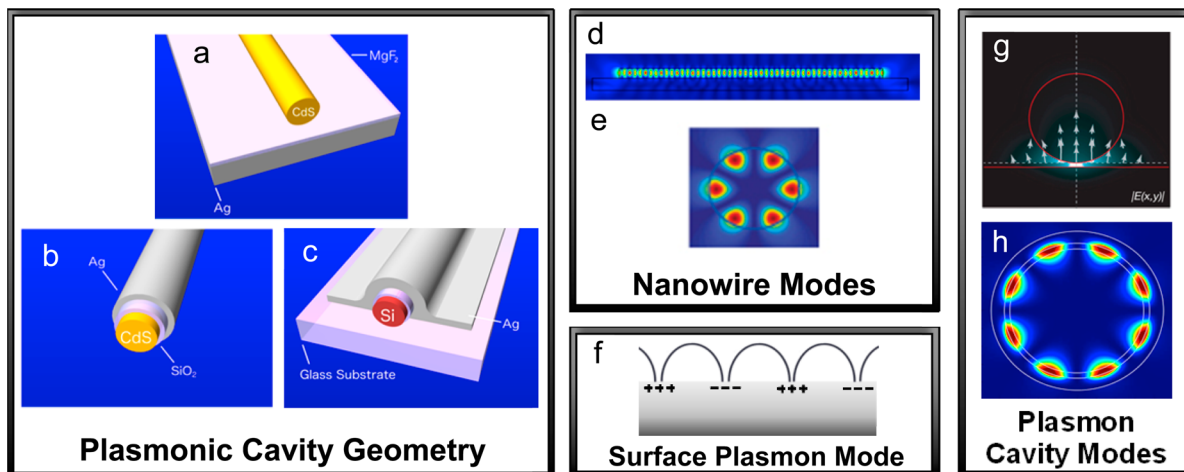


Figure 1. Various concepts for integration of semiconductor NWs with plasmonic nanocavities and the associated optical modes. (a–c) Schematic of integration of NWs with plasmonic nanocavities in (a) NW-on-planar insulator–metal, (b) core–shell NW–insulator–metal, and (c) Ω-shaped NW–insulator–metal geometries. (d,e) Computational electromagnetic simulation of (d) an all-dielectric CdS NW longitudinal waveguided mode⁷⁶ and (e) Ge NW WGM resonance.⁶³ (f) Schematic of a surface plasmon mode on a planar metal film. (g,h) Plasmonic modes resulting at the interface of a semiconductor NW with (g) a metal film²⁹ and (h) a core–shell CdS–Ag cavity.²⁶ Copyright 2009 Nature Publishing Group.^{29,63} Copyright 2011 Nature Publishing Group.²⁶ Copyright 2013 Nature Publishing Group.²⁷ Copyright 2011 Proceedings of the National Academy of Sciences.⁷⁶

Interestingly, each system employs a different type of NW mode, modes that propagate along the NW long axis (waveguided modes, Figure 1d) and those that propagate in the plane of the cross section (WGM resonances, Figure 1e), which, when hybridized with the surface plasmon mode of a nearby metallic nanostructure, will result in various hybrid modes and functionalities (Figure 1g, h). We begin with the system outlined in Figure 1a, where a CdS NW (with diameter $d = 50\text{--}400\text{ nm}$) is interfaced with a thick silver film but separated from the metal surface with a $\sim 5\text{ nm}$ insulating layer (MgF_2).²⁹ The insulating gap is critical in terms of both the quantum yield of the optical emitter and the electromagnetic modes involved. As discussed above, the proximity of an optical emitter to a metal surface can also quench the emission due to excitation of high-order nonradiative modes in the metal^{36,78} or direct electronic energy transfer between the metal surface and charge carrier at small distances of a few nm.^{78,79} In contrast, the charge carrier excitation rate will also increase asymptotically with decreasing separation from the metal, as shown by Anger et al., leading to an optimized separation of $\sim 5\text{ nm}$ between the optical emitter and metal to achieve maximal enhancement of the quantum yield.³⁶ Perhaps even more critical are the new hybridized electromagnetic modes that are enabled by the thin insulating gap. By using a low refractive index gap, Oulton et al. demonstrated, through finite element analysis, that a significant portion of the field is stored near this optically lossless insulating region.⁸⁰ The waveguided modes are plasmonic in nature and confined to deep-subwavelength dimensions of $\sim 10^{-2}\lambda$ near the metal surface, yet a majority of the field is guided outside of the lossy metal in the insulating gap that enables waveguiding over longer distance ($>10\text{ }\mu\text{m}$). The large fields inside of the low index gap layer can be understood in terms of continuity of the displacement current at the interface between two materials, which demands a high normal component of the electric field in the low index region, thus enabling the gap layer to behave like a capacitor for the field. Furthermore, using coupled mode theory, the new hybrid modes can be modeled as a superposition of the NW and surface plasmon modes,⁸⁰ highlighting

the potential synergy between these two types of electromagnetic modes.

Returning to the CdS–MgF₂–Ag system, hybrid NW/surface plasmon modes were excited via the photoluminescence from the plasmonically coupled CdS NW (Figure 2a). The low mode volumes associated with the hybrid modes in conjunction with modal overlap in the CdS gain medium result in plasmon-enhanced laser action from CdS (Figure 2b) at the CdS I₂ exciton line. More importantly, for small NWs with $d < 150\text{ nm}$, the photonic CdS NW, that is, a NW that is not interfaced with a plasmonically active metal, does not exhibit lasing due to decreasing mode confinement and thus poor overlap with the gain medium. This effect was also demonstrated in studies of waveguided modes in bare ZnSe NWs where single-mode operation was shown at NW diameters as small as $\lambda/9$ but with increasing leakage of the mode outside of the NW with decreasing diameter.⁶⁵ Indeed, the pump thresholds required for lasing diverge for uncoupled NWs with diameters below $\sim 150\text{ nm}$, with the plasmonic system requiring significantly lower threshold intensity (Figure 2c) down to $d \approx 50\text{ nm}$, the experimental limit of the sample size distribution. The plasmonically coupled CdS NW is also associated with about a ~ 6 times faster spontaneous emission rate (see Figure 2d), as expected from the previous discussion on active media interfaced with plasmonically active materials (i.e., metals such as Au or Ag with plasmon resonances in the visible range). It should be noted that in addition to lasing from CdS below the photonic “cutoff”, the polarization of the laser light in the plasmonic system is that of the surface plasmon mode, that is, parallel to the NW long axis. The lasing emission polarization matches that of the hybrid mode and is orthogonal to the polarization of lasing from photonic NWs as the photonic modes involved also have polarization perpendicular to the NW long axis.

Until this point, integration of semiconductors with surface plasmons has focused on either open geometries such as metal films and metal NWs, which host SPP modes, and metal nanostructures, which host LSPs. Resonant optical cavities based on surface plasmon modes, on the other hand, should yield the

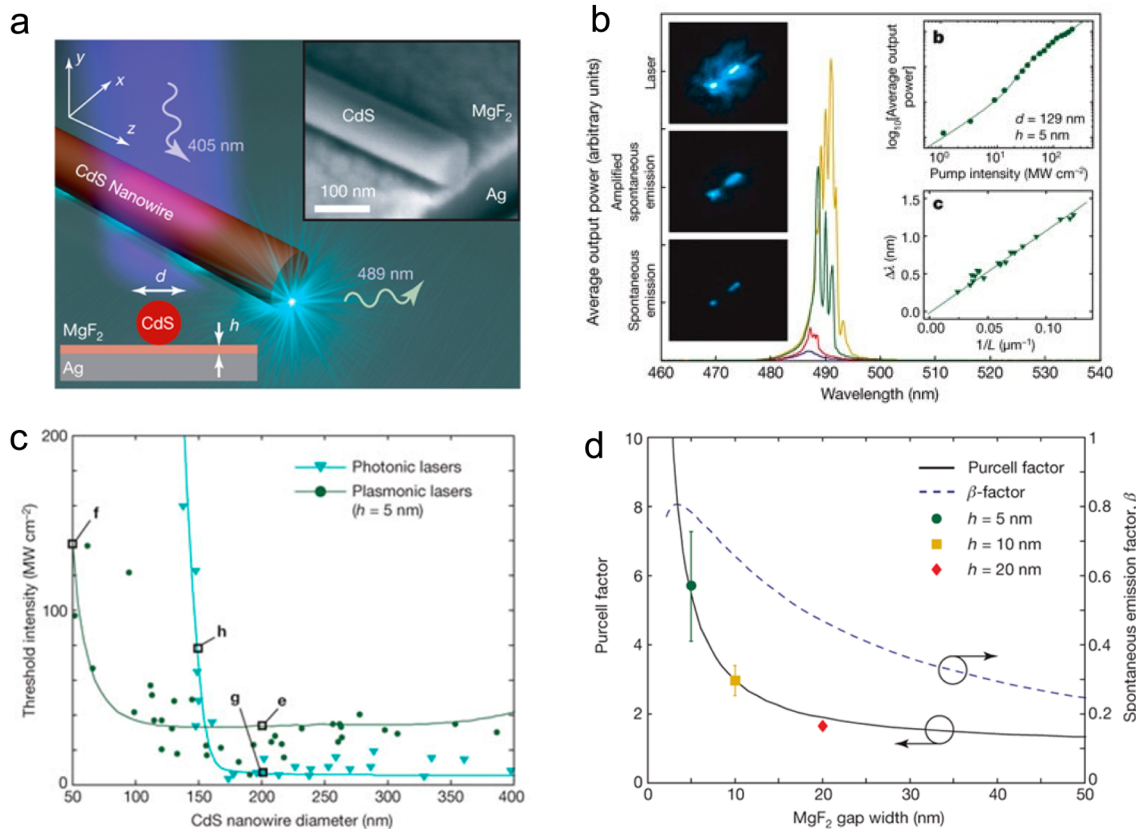


Figure 2. Lasing from a CdS NW interfaced with a Ag film. (a) Schematic of plasmonically coupled CdS in the NW–insulator–Ag film geometry (inset: SEM micrograph). (b) Photoluminescence spectrum of plasmonically coupled CdS demonstrating lasing action at the I₂ exciton line. (Inset: (left) transition from spontaneous emission to lasing; (right) power dependence of emission and mode spacing versus length corresponding to an effective index of 11). (c) Threshold intensity versus NW diameter demonstrating lasing in plasmonically coupled CdS below the photonic lasing cutoff. (d) Purcell enhancement for plasmonically coupled CdS. Copyright 2009 Nature Publishing Group.²⁹

sought-after combination of both (reasonably) high Q modes due to their closed architecture and low mode volumes normally associated with surface plasmon modes. Using a core–shell resonant cavity architecture (Figure 1b), Cho et al. demonstrated very large Purcell factors of $\sim 10^3$ in CdS NWs based on spectral overlap between the SPP modes of the plasmonic nanocavity and electronic resonances in CdS.²⁶ Furthermore, this technique was extended to an indirect band gap semiconductor material, silicon, leading to similar high Q/V_m values.²⁷ With Purcell enhancements at this extreme level, the spectroscopic properties of both material systems are significantly altered and will be discussed below.

In a direct band gap semiconductor (e.g., CdS, with significant ionic character), intraband relaxation of the carriers occurs via scattering with longitudinal-optical (LO) phonons and acoustic phonons in approximately 0.1 and 100 ps, respectively.⁸¹ The conduction band minimum at $k = 0$ is resonant with the light line (i.e., the photon dispersion, $\omega = ck$) at $k \approx 0$; thus, the photon state is both energy- and momentum-matched to the electronic state at $k \approx 0$, and the electron may recombine radiatively with a hole (Figure 3a, blue curves). This radiative recombination process typically occurs on a nanosecond time scale and is generally much slower than the intraband relaxation processes (~ 1000 times slower in this case).^{81,82} This difference in time scales explains why CdS and other semiconductor materials mostly emit from the ground state (band edge) under normal conditions. This phenomenon is well-known in

photochemistry, where it has been described by “Kasha’s Rule”⁸³

We note that in all of the references on surface-plasmon-enhanced spontaneous emission discussed thus far, light emission is restricted to near the band edge, again due to the time scales of intraband relaxation and radiative recombination. On the other hand, if Purcell enhancement and thus the spontaneous emission rate can be increased by a factor of 10^2 – 10^3 , then in principle, radiative recombination can become competitive with the intraband relaxation process, which is typically ~ 1000 times faster. In order to explore Purcell enhancement in a semiconductor NW integrated with a resonant plasmonic optical cavity, Cho et al. fabricated a conformal CdS–SiO₂–Ag core–shell NW system (Figure 1b) where the SiO₂ interlayer serves three important functions; first, it serves to prevent quenching of excited charge carriers by the metal and plays a key role in developing the hybrid electromagnetic modes of the system as explained in the studies of Oulton et al.²⁹ In addition, deposition of a SiO₂ layer on CdS has been established as a method to prevent exciton scattering at the sample surface due to the chemical passivation of dangling bonds at the surface, where it was shown that after passivation with SiO₂, light emission from CdS NWs is dominated by free exciton recombination.⁸⁴ Furthermore, in these experiments, we do not observe radiative recombination from excitons at the surface, which occurs at energies below the band edge. The photoluminescence spectrum of a SiO₂-coated CdS NW is shown in Figure 3b (blue curve) and demonstrates free A and B exciton

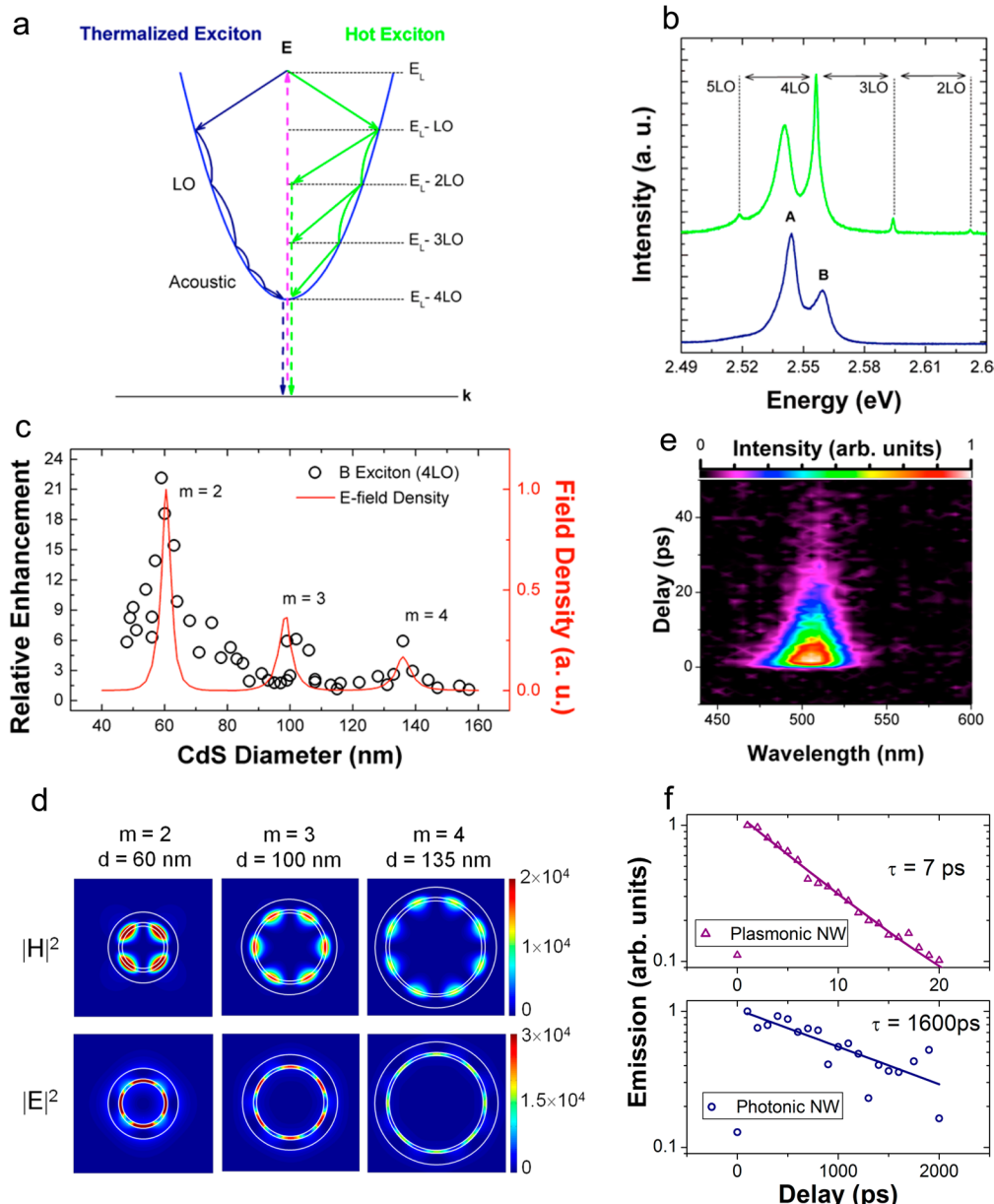


Figure 3. Hot luminescence from a plasmonically coupled CdS NW in a core–shell architecture. (a) Schematic of exciton generation (dashed magenta line), relaxation, and the emission process for a “normal” or thermalized exciton (blue curves, left) and also for a nonthermalized or hot exciton (green curves, right) in CdS, a direct band gap semiconductor. E_L marks the energy of the exciting laser. (b) Photoluminescence spectra for a bare CdS NW (blue curve, bottom) and plasmonically coupled NW (green curve, top) demonstrating the hot exciton emission process explained in (a). The bare CdS NW shows emission from thermalized excitons only. (c) Size-dependent enhancement of a 4LO hot exciton (resonant with B-exciton) photoluminescence peak (open circles) in plasmonically coupled CdS NWs and the calculated field intensity per unit area (red curve) as a function of NW diameter. (d) FDTD simulations of magnetic field ($|H|^2$) and electric field ($|E|^2$) intensity profiles for plasmonically coupled NWs at the three resonant sizes $d = 60$ ($m = 2$ corresponds to the azimuthal mode order), 100 ($m = 3$), and 135 nm ($m = 4$) observed in the size-dependent spectra in (c). (e) Time-resolved photoluminescence spectral map measured from an ensemble of 300–500 NWs with an average diameter of 140 ± 50 nm taken at room temperature (300 K). (f) Time-resolved integrated photoluminescence emission intensity for plasmonically coupled (upper) and bare (lower) CdS NWs. Solid lines are an exponential fit to the data. The resulting fits yield radiative recombination lifetimes of 7 and 1600 ps for the plasmonically coupled and bare CdS NWs, respectively. Copyright 2011 Nature Publishing Group.²⁶

emission (thermalized) in CdS.⁸⁵ Upon addition of a conformal metal shell, there is an increase in the overall photoluminescence intensity (after taking into account in- and out-coupling efficiencies).²⁶ Interestingly, the spectral shape now features sharp peaks at multiples of the LO phonon energy in CdS (~ 38 meV⁸⁶) from the laser excitation energy above the band edge, which suggests that LO phonon scattering now serves to both mediate carrier relaxation and also scatter the

carrier back to the light line (Figure 3a, green curve), leading to emission from unthermalized (hot) charge carriers. However, the most interesting thing is that in a steady-state spectrum, emission from states that are very short lived (on the order of the exciton–LO phonon interaction time scale, i.e., a few ps) is observable, which strongly suggests that the radiative lifetime of the cavity is becoming comparable to the LO phonon interaction time scales due to the Purcell effect.

The most intense peak in Figure 3b corresponds to resonance between the ground state (B-exciton) and hot state at an energy corresponding to 4LO phonons below the energy of the excitation laser. The relative enhancement of this peak features a dependence on the NW diameter, which when plotted against the NW size (Figure 3c, open circles) demonstrates an overall increase with decreasing NW diameter that is also punctuated by several peaks. Finite difference time domain (FDTD) simulations reveal highly confined SPP modes in direct analogy to those of all-dielectric WGM resonators,^{7,87} that is, with the k vector in the angular direction only but confined to the region near the Ag–CdS interface (Figure 3d). As can be observed from the frequency domain electric field intensity profiles, as the diameter of the CdS core decreases, the electric field density increases (Figure 3c, red curve), which closely follows the increase in hot luminescence yield. Furthermore, Purcell factors may be computed directly from the computational electromagnetic data, which yield Purcell factors on the order of $\sim 10^3$. Of note is the extremely small mode volume associated with these modes, which is $10^{-4}\lambda_0^3$, where λ_0 is the vacuum wavelength. In other words, light in these cavities is 10 000 times more confined than that in free space, which, when coupled with moderate quality factors ($Q \approx 50$), leads to the exceptionally high Purcell enhancements. A near-complete transition from thermalized luminescence to hot luminescence is further corroborated by time-resolved photoluminescence spectroscopy, which shows a transition from a 1.6 ns lifetime in bare CdS to 7 ps in the plasmonically coupled samples (Figure 3e,f). Perhaps more impressive is the fact that these are ensemble measurements made on CdS NWs with significant spread in their size distribution, that is, the measured sample had an average diameter of $d = 140 \pm 50$ nm (and typical lengths of 10–20 μm); thus, even lower emission lifetimes are expected on the single NW level at the “resonant sizes”, in this case, $d = 60, 100$, or 135 nm, which are the dimensions where the SPP-WGM mode is spectrally matched to the emission (see Figure 3c).²⁶ To summarize, by interfacing a direct band gap material (e.g., CdS) with an appropriately designed optical antenna or plasmonic cavity, the spontaneous emission rate was enhanced to the point where it became competitive with intraband relaxation processes to enable emission predominantly from unthermalized (hot) states, an interesting finding from a spectroscopic point of view. From a device physics perspective, on the other hand, this implies that that NW optical and optoelectronic devices may be modulated at orders of magnitude higher frequency by interfacing the active material with an appropriate plasmonic cavity. Furthermore, there is no immediate impediment as to why the metal could not double as a channel for charge injection and extraction, leading to compact device geometries.

On the other hand, in terms of making more efficient light emitters, CdS is not the appropriate material as its quantum yield is already high.⁸⁸ Materials that would benefit from highly enhanced spontaneous emission would be “dark” materials, that is, indirect band gap semiconductors, which convert energy to heat much more readily than to light.⁸⁹ In fact, light-emitting materials often feature a decrease in their quantum yield when they are interfaced with plasmonically active materials due to nonradiative processes. Materials with low intrinsic quantum yield, on the other hand, will generally feature an increase in their quantum yield due to the comparatively high increases in radiative decay rate, given proper optimization of the active media–metal architecture.¹⁹

Silicon is perhaps one of the most important of the indirect band gap semiconductor materials due to its ubiquity in the semiconductor electronics industry. Silicon combines a suite of attractive physical properties; it is mechanically robust, conductive, nontoxic, and abundant, and as such, the semiconductor industry has spent decades perfecting Si processing techniques. Yet one of the key properties missing in Si is efficient light emission in the visible range. In Si, once the electron is excited to the conduction band (typically by a phonon-assisted process), its behavior is quite similar to that of an excited charge carrier in the direct band gap semiconductor. The excited electron will quickly relax to the conduction band minimum via phonon scattering events that occur on a 0.1–1 ps time scale (i.e., intraband relaxation).^{90–92} The key difference with a direct band gap material like CdS is that in an indirect band gap material such as silicon, once the electron reaches the conduction band minimum (near the X and L points), it is momentum-mismatched from the valence band maximum at the Γ point (Figure 4a); thus, in order for an electron to recombine radiatively with a hole, it must exchange momentum with the crystal lattice, which is an inefficient process due to the lack of availability of large wave vector phonons. Unlike in CdS, here, the emission quantum yield is $\sim 10^{-6}$ at the conduction band minimum⁸⁹ and estimated to be 10^{-4} near the direct band gap.²⁷ In Si, the relaxed carrier is much more likely to lose its energy via several nonradiative processes such as recombination at defect sites (impurity states),⁹³ free carrier absorption,⁹³ and Auger recombination.⁹⁴ Obtaining efficient light emission from silicon via highly enhanced radiative recombination is a logical route given that the farther the excited carrier intraband relaxes toward the conduction band minimum, the less probable it is to find phonons of the appropriate momentum to enable radiative recombination at the light line ($k \approx 0$). In CdS, the hot luminescence associated with high Purcell enhancements (10^2 – 10^3) resulted in emission from electronic states, which were not thermalized (that is, not yet at the conduction band minimum) and where the hot luminescence process was mediated by scattering with LO phonons²⁶ (with which electrons in CdS have high coupling factors^{5,88}). The same principle may be applied in Si if interfaced with a properly designed plasmonic nanocavity. Moreover, Si benefits from having several regions in its phonon dispersion that are nearly flat, that is, having a very high density of states.²⁷ These phonons can mediate the hot luminescence process and would serve to scatter carriers from the electronic branch to the light line.

Cho et al. interfaced Si NWs with a plasmonic nanocavity in a “Ω-shaped” geometry (Figure 1c) assembled on a glass substrate followed by a thin coating of an insulating SiO_2 spacer layer for reasons discussed above.²⁷ Metallization from the top results in the Ω cavity, which sustains electromagnetic modes that are WGM-type, that is, propagate in the cross section of the NW but are close to the metal–dielectric interface. We note that in this case, Si benefits from the broken symmetry at the base of the cavity where the Si NW is interfaced with the substrate as it is no longer subject to the periodic boundary condition²⁶ and can therefore sustain half-integer multiples of the wavelength around the periphery of the Si NW.

Photoluminescence measurements on Si NWs without the Ω cavity resulted only in a background level signal, as demonstrated in Figure 4b (blue curve). Addition of the plasmonic nanocavity results in broad-band emission across the visible spectrum (Figure 4b, green curve) and a quantum yield of 1.4%, which represents at least 2 orders of magnitude enhancement

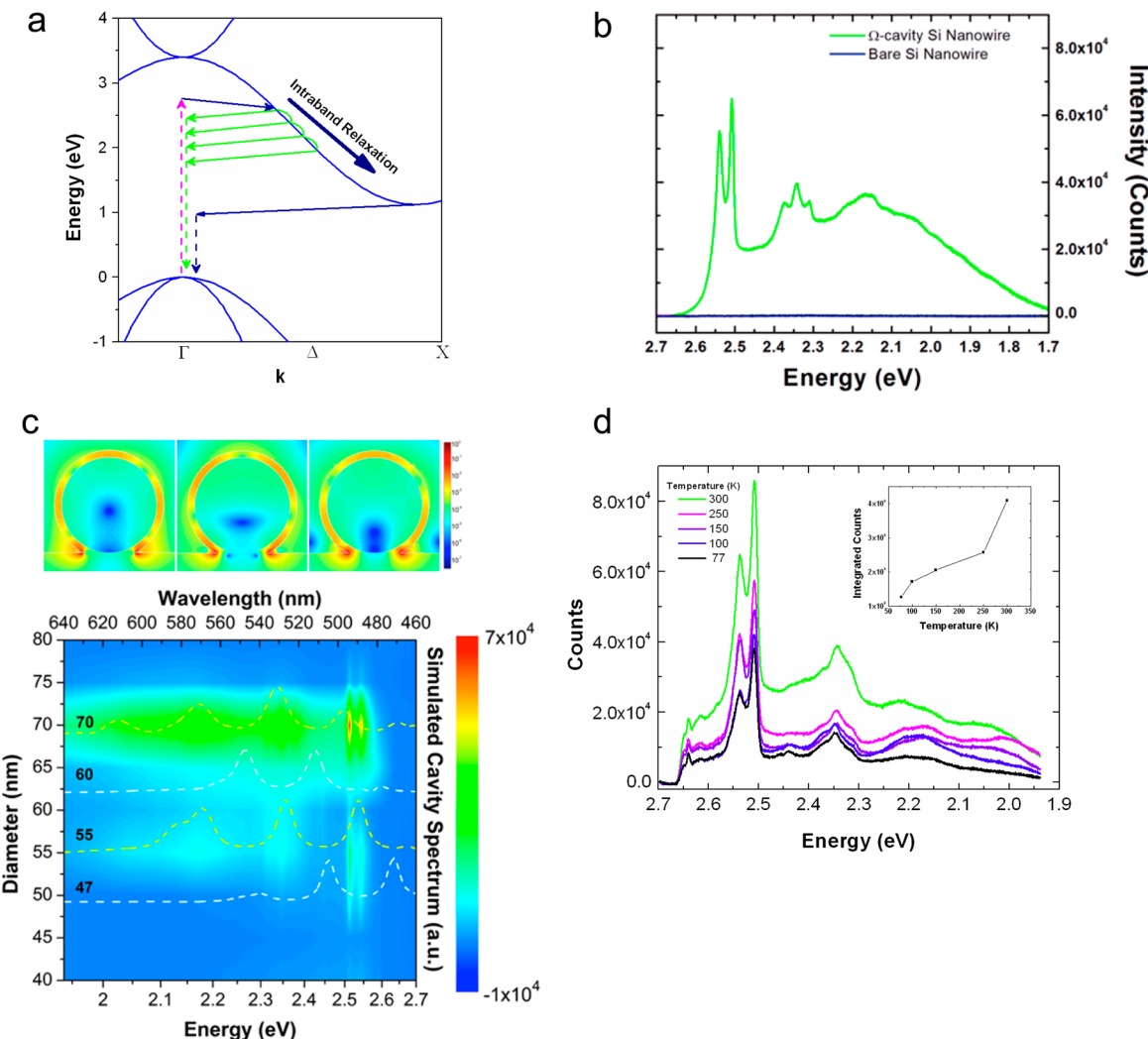


Figure 4. Hot luminescence from plasmonically coupled Si NW in the Ω cavity architecture. (a) Diagram of charge carrier generation, relaxation, and emission in Si for a carrier thermalized to the conduction band minimum (blue curves) and a nonthermalized (hot) carrier (green curves). (b) Photoluminescence spectrum of bare Si (blue curve) and plasmonically coupled Si (green curve) NWs. (c, top) Frequency domain electric field intensity ($|E|^2$) profiles for plasmonic cavity modes in Si NW coupled with the Ω cavity. (c, bottom) Plot of size-dependent photoluminescence spectra of plasmonically coupled Si NW for sizes in the range of $d = 40\text{--}80\text{ nm}$. Simulated cavity spectra are superimposed (dashed curves) for select sizes denoting nonresonant cases ($d = 47$ and 60 , dashed white curves) and resonant cases ($d = 55$ and 70 nm , yellow curves). (d) Temperature-dependent photoluminescence spectra of plasmonically coupled Si NWs for temperatures in the range of $77\text{--}300\text{ K}$, demonstrating a positive temperature dependence, which confirms a hot photoluminescence process and is opposite that of a resonant-Raman process. Copyright 2013 Nature Publishing Group.²⁷

compared to the emission yield near the direct band gap.²⁷ FDTD simulations reveal highly confined cavity modes, which span the visible range (Figure 4c, top). Size-dependent simulations further demonstrate that the emission intensity is highest when the SPP modes are resonant with highly efficient phonon-mediated emission channels, that is, in the case of the $d = 55$ and 70 nm NWs (Figure 4c). We remind the reader that quality factors of the modes hosted by these nanoscale optical cavities ($<10^2$) are low compared to their micron-scale all-dielectric counterparts ($>10^4$),⁹⁵ yet it is the very low mode volumes (in this case, 10^{-4} that of light in free space) that result in even higher values of Q/V_m . Furthermore, there are significant advantages with working low Q modes (discussed above) that enable enhancement of spontaneous emission over a large spectral range.

Finally, we note an important caveat of the investigations on hot photoluminescence discussed thus far. Hot photoluminescence has similar spectral characteristics to resonant-Raman

scattering, such as peaks that occur at fixed phonon energies from the laser line, even though hot luminescence and resonant-Raman scattering are fundamentally different processes where the former involves real electronic transitions whereas the latter does not.⁹⁶ Extensive studies on plasmonically coupled Si NWs strongly suggest that the light emission mechanism is from hot photoluminescence.⁸⁷ For this Perspective, we highlight the positive temperature dependence of the emission (Figure 4d) that demonstrates increasing luminescence intensity indicative of an indirect emission process⁹⁸ and which is opposite that of direct band gap emission⁹⁹ and several other relevant Raman scattering processes.^{100,101} For further discussion and more detailed spectroscopic analysis, we refer the reader to the recent study by Asperti et al.⁹⁷

We also note the implication that modes that enable significant light emission should also enable large enhancements in absorption, another important optical property of materials,

and should serve to produce devices that are highly enhanced optical antenna absorbers. Engineering of absorption in semiconductor NWs has been pursued via the WGM resonances of NWs^{63,71} and LSP modes of randomly dispersed metal nanoparticles on semiconductor NWs,¹⁰² yet the effects of plasmonic cavity resonances have yet to be analyzed in the context of enhanced absorption, which is examined below.

In general, absorption in semiconductor NWs is dictated by the polarization of incoming light and the dielectric mismatch that exists between the high refractive index NWs and their surroundings. In the absence of electromagnetic resonances, it has been demonstrated that semiconductor NWs absorb light that is polarized parallel to the long axis of the NW much more readily than light that is polarized perpendicular to its axis (in the plane of the cross section) due to the dielectric mismatch.¹⁰³ The modes that are polarized parallel to the NW long axis are typically termed “TM” or transverse magnetic, and those that are polarized perpendicular to the NW long axis are “TE” or transverse electric.^{63,102} The polarization-dependent absorption anisotropy, which is observed in bare semiconductor NWs when the diameter is small compared to the wavelength of the incoming light, is orthogonal to that of semiconductor NWs integrated with a plasmonic nanocavity discussed above (core–shell geometry). Boundary conditions on SPP modes dictate that their electric field polarization must be in the direction of propagation.¹² Thus, for surface plasmon modes in the plane of the NW cross section, we expect TE polarized light to play a significant role in the absorption characteristics of the semiconductor NW, traditionally dominated by TM polarized light in bare (photonic) NWs.¹⁰³

The absorption properties of both CdSe and Ge NWs are highlighted for this Perspective. CdSe is chosen due to the similarity in its dielectric properties to CdS but with a lower band gap (1.74 eV) that enables absorption across the visible spectrum. Ge, on the other hand, is an indirect band gap semiconductor with electronic and optoelectronic applications.^{63,104,105} The simulated absorption spectrum of a bare CdSe NW (diameter $d = 60$ nm) is shown in Figure 5a, presented as % absorbed power normalized to the source power of a diffraction-limited Gaussian beam. The specifications of the excitation source are chosen to match a typical laser lab setup. As expected in this subwavelength NW size range, TM polarized light dominates the absorption spectra due to the much higher dielectric mismatch experienced by TE polarized light and approaches zero absorption below the CdSe band gap due to the lack of electronic states at lower energies. Absorption of TE polarized light demonstrates a monotonic decrease with increasing wavelength (Figure 5a, red curve) due to the lack of any optical resonances and due to the increasing effect of spatial dielectric mismatch with increasing wavelength of the incident light. Addition of a conformally coated thin (15 nm) silver layer on the CdSe NW (Figure 1b), on the other hand, reverses the polarization dependence of the absorption spectrum, where the absorption is now dominated by the TE polarized light (Figure 5b, red curve) albeit at the expense of absorption due to TM polarized light (Figure 5b, blue curve). Interestingly, by placing what is essentially a mirror on the active material, we would expect a decrease in light absorption all along the active layer (in this case, the CdSe NW), but by utilizing a thin Ag film on the order of the skin depth, the system is able to host surface plasmon modes, which transform this system into an optical antenna, capable of concentrating far-field light into the NW core (Figure 5c). Here, the absorption spectrum is punctuated

by the dipolar surface plasmon resonance (centered at ~690 nm) and a higher-order mode centered at ~480 nm. Absorption in the metal-coated NW due to TM radiation is mediated by the fundamental first-order WGM mode resonance (Figure 5d) and can be exploited to achieve increases in absorption to levels even higher than the photonic case (discussed later). Furthermore, the resonances are highly tunable (Figure 5e), demonstrating a blue shift with increasing Ag shell thickness in line with that reported for core–shell metal–semiconductor nanoparticles.¹⁰⁶ It should be noted that the bare and core–shell NWs were simulated in two dimensions, which is reasonable given that the SP modes in core–shell semiconductor–metal NWs do not propagate along the NW long axis and are confined to the cross section only.

Similar studies were conducted on Ge, which is generally used as an electronic (as opposed to optical) material, as discussed above. The characteristics of the absorption spectrum of a bare Ge NW, $d = 40$ nm (Figure 5f), are similar to those of CdSe but with the spectrum extending to the near-IR due to the lower band gap of Ge (0.67 eV). We note that for CdSe, 15 nm is the smallest thickness of the Ag shell possible, before the dipolar surface plasmon resonance is pushed below the CdSe band gap (as demonstrated for a CdSe NW coupled with a 10 nm Ag shell; Figure 5e, red curve). In the case of Ge, which exhibits a lower-energy band gap, addition of a 10 nm Ag coating yields broad-band enhancement not only of the absorption of TE polarized light (Figure 5g, red curve) but also of the absorbed TM polarized light (Figure 5g, blue curve) in comparison to the bare Ge NW. Again, the TE spectrum is mediated by the strong dipolar surface plasmon resonance (Figure 5h). Furthermore, we note that by choosing a smaller NW ($d = 40$ nm compared to 60 nm for CdSe), we are able to tune the resonances to the visible range, which highlights the tunability of these resonances as a function of NW dimensions. Again, TM absorption is dominated by the lowest-order WGM mode (Figure 5i). In this case, absorption of TM polarized light is enhanced across the entire spectrum and to levels higher than that of the bare Ge NW. We expect that the broad-band enhancement of the TM absorption is due in part to the high refractive index of Ge coupled with limited radiative losses, which are achieved by placing a metal around the NW. Although for the TM case this is not a surface plasmon mode per se, using metals to limit radiative losses of photonic modes is a known technique that leads to increased photonic confinement.^{107–109} As highlighted in the studies of absorption in NWs composed of both direct band gap (CdSe) and indirect band gap (Ge) semiconductor materials, surface plasmon cavities can be used to engineer not only the light emission properties but also light absorption. We expect highly tunable absorption in plasmonically coupled semiconductors to have direct applications in photodetectors and photovoltaics.

Returning to our exposition on spontaneous emission enhancement in semiconductor nanowires, we expect this type of plasmonic cavity engineering to play an important role in future photonic and optoelectronic devices as we may now build devices where light emission and absorption are not dictated only by material properties but also by optical engineering of hybrid semiconductor–metal systems. In other words, the techniques discussed here provide a method to tune both the wavelength and rate of the emission in active materials. Moreover, the systems highlighted in this Perspective are amenable to length scales of current lithographic techniques.

Surface-plasmon-based lasing has already lent itself to produce truly nanoscopic sources of light⁵¹ that is both temporally

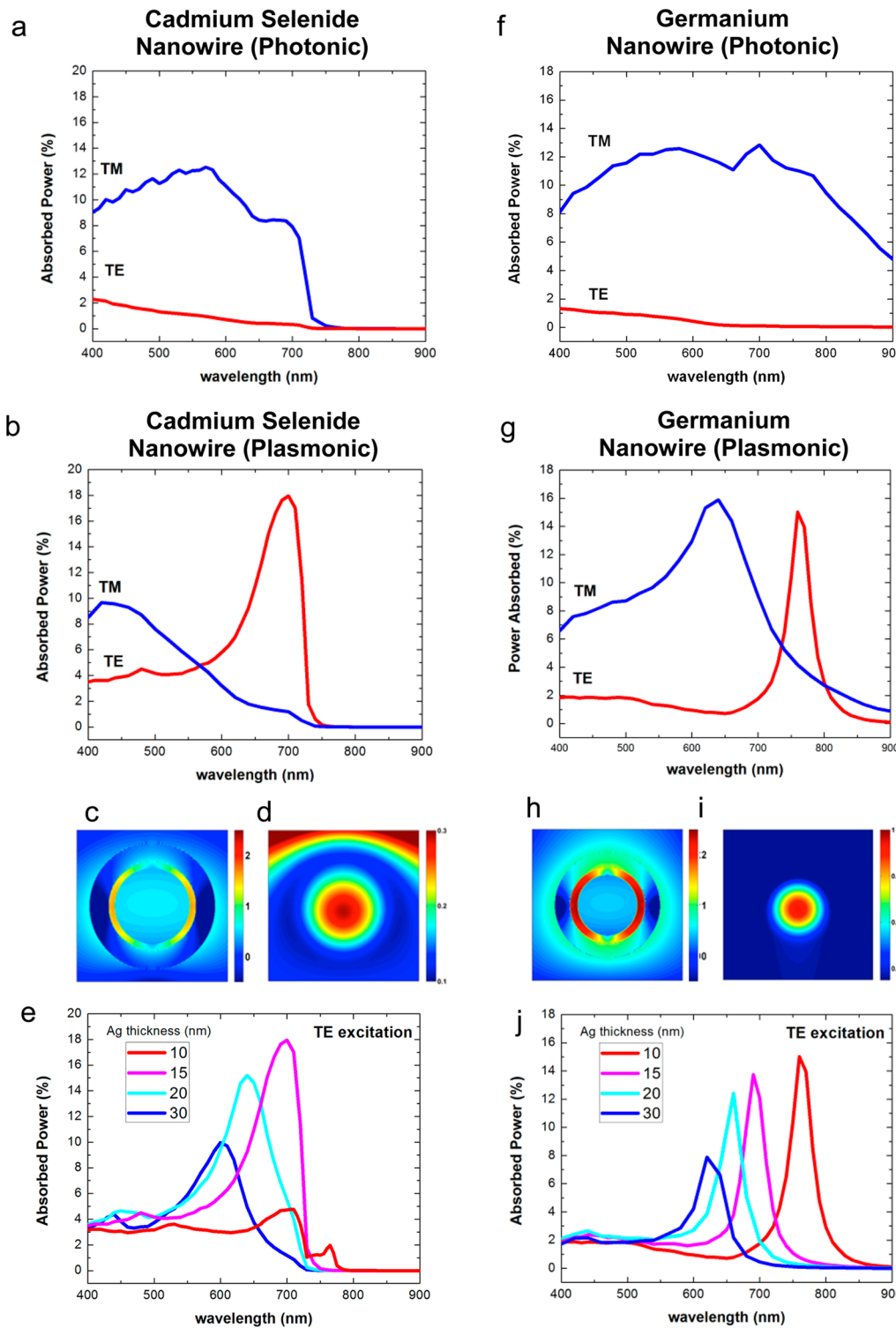


Figure 5. Demonstration of enhanced absorption in plasmonically coupled, core–shell CdSe–Ag and Ge–Ag NWs (following the core–shell semiconductor–metal architecture presented in Figure 1b) via FDTD simulations. (a,b) Simulated absorption spectrum of a bare CdSe NW (a) and a core–shell CdSe–Ag NW (b) featuring absorption of TM polarized light (blue curve) and TE polarized light (red curve). (c) Frequency domain electric field intensity ($|E|^2$) profile of dipole surface plasmon resonance in core–shell CdSe–Ag NWs due to TE excitation in plasmonically coupled CdSe (log scale). (d) Frequency domain electric field intensity ($|E|^2$) profile of the fundamental WGM resonance in core–shell CdSe–Ag NWs due to TM excitation (linear scale). (e) Absorption spectra of core–shell CdSe NWs under TE excitation with varying Ag shell thicknesses (in the range of 10–30 nm). (f,g) Simulated absorption spectrum of bare Ge NWs (f) and core–shell Ge–Ag NWs (g) featuring absorption of TM polarized light (blue curve) and TE polarized light (red curve). (h) Frequency domain electric field intensity ($|E|^2$) profile of dipole surface plasmon resonance due to TE excitation in core–shell Ge–Ag NWs (log scale). (i) Frequency domain electric field intensity ($|E|^2$) profile of the fundamental WGM resonance in core–shell Ge NWs due to TM excitation (linear scale). (j) Simulated absorption spectra of core–shell Ge–Ag NWs under TE excitation with varying Ag shell thicknesses (in the range of 10–30 nm).

Returning to our exposition on spontaneous emission enhancement in semiconductor nanowires, we expect this type of plasmonic cavity engineering to play an important role in future photonic and optoelectronic devices as we may now build devices where light emission and absorption are not dictated only by material properties but also by optical engineering of hybrid semiconductor–metal systems.

and spatially coherent due to the small, subdiffraction-limited volumes. As optoelectronic devices become ever more densely packed, we expect power consumption of nanoscopic light sources to play a key role. Thus, future research will likely focus, in part, on developments that improve modal overlap between the low-mode volume optical antenna modes and gain media⁴¹ and reduce ohmic losses in the metal,^{29,49} thereby reducing laser thresholds and power consumption. Furthermore, the ability to readily synthesize NW heterostructures⁵⁹ in tailored chemical compositions⁶¹ facilitates fabrication of NW p–n junctions.⁵⁹ This is an essential component for electrically pumped plasmonic NW devices, where, as mentioned above, the metal component may serve as both an optical cavity and a source of charge injection and extraction.

We also acknowledge notable efforts to produce nanoscale lasers in solid-state metallocodielectric systems operating close to the diffraction limit.^{107,108} In this case, a metal cladding is used to lower radiative loss of cavity modes, thereby lowering laser thresholds and promoting laser action. Although this technique does not rely on plasmonic modes, we expect this type of cavity confinement to enhance the optical resonances inherent to semiconductor NWs, which will lend itself to promoting both lasing and perhaps novel nonlinear optical effects.

AUTHOR INFORMATION

Corresponding Author

*E-mail: riteshag@seas.upenn.edu.

Notes

The authors declare no competing financial interest.

Biographies

Dr. Carlos O. Aspetti is a recent alumni of the Agarwal group at Penn. His thesis work, entitled “Surface Plasmon Based Engineering of Semiconductor Nanowire Optics”, is the basis for a significant portion of the work presented in this Perspective. He is currently working in the commercial sector as a management consultant.

Ritesh Agarwal is a Professor of Materials Science and Engineering at Penn, with research interests in nanophotonics, including understanding and engineering light–matter interactions in one- and two-dimensional semiconductors and studying nanoscale phase transitions and electronic memory switching. He is the recipient of the NSF CAREER (2007), NIH Director’s New Innovator Award (2010), and the SPIE Symposium Nanoengineering Pioneer award (2014). <http://agarwal.seas.upenn.edu>

ACKNOWLEDGMENTS

This work was supported by the U.S. Army Research Office under Grants W911NF-09-1-0477 and W911NF-11-1-0024 and the National Institutes of Health through the NIH Director’s New Innovator Award Program, 1-DP2-7251-01. C.O.A. is supported by the United States Department of Defense, Air Force Office of Scientific Research, National Defense Science and Engineering Graduate (NDSEG) Fellowship.

REFERENCES

- (1) Hecht, E. *Optics*, 4th ed.; Addison-Wesley: Reading, MA, 2001.
- (2) Purcell, E. M. Spontaneous Emission Probabilities at Radio Frequencies. *Phys. Rev.* **1946**, *69* (11–1), 681–681.
- (3) Ryu, H. Y.; Notomi, M. Enhancement of Spontaneous Emission from the Resonant Modes of a Photonic Crystal Slab Single-Defect Cavity. *Opt. Lett.* **2003**, *28*, 2390–2392.
- (4) Giannini, V.; Fernandez-Dominguez, A. I.; Heck, S. C.; Maier, S. A. Plasmonic Nanoantennas: Fundamentals and Their Use in Controlling the Radiative Properties of Nanoemitters. *Chem. Rev.* **2011**, *111*, 3888–3912.
- (5) Adachi, S. *Properties of Group-IV, III–V and II–VI Semiconductors*; Wiley: New York, 2005.
- (6) Peter, E.; Senellart, P.; Martrou, D.; Lemaître, A.; Hours, J.; Gérard, J. M.; Bloch, J. Exciton–Photon Strong-Coupling Regime for a Single Quantum Dot Embedded in a Microcavity. *Phys. Rev. Lett.* **2005**, *95*, 067401.
- (7) Armani, D. K.; Kippenberg, T. J.; Spillane, S. M.; Vahala, K. J. Ultra-High-Q Toroid Microcavity on a Chip. *Nature* **2003**, *421*, 925–928.
- (8) Vahala, K. J. Optical Microcavities. *Nature* **2003**, *424*, 839–846.
- (9) Vernooy, D. W.; Furusawa, A.; Georgiades, N. P.; Ilchenko, V. S.; Kimble, H. J. Cavity QED with High-Q Whispering Gallery Modes. *Phys. Rev. A* **1998**, *57*, R2293–R2296.
- (10) Vollmer, F.; Braun, D.; Libchaber, A.; Khoshima, M.; Teraoka, I.; Arnold, S. Protein Detection by Optical Shift of a Resonant Microcavity. *Appl. Phys. Lett.* **2002**, *80*, 4057–4059.
- (11) Burke, J.; Stegeman, G.; Tamir, T. Surface-Polariton-Like Waves Guided by Thin, Lossy Metal Films. *Phys. Rev. B* **1986**, *33*, 5186–5201.
- (12) Maier, S. A. *Plasmonics: Fundamentals and Applications*; Springer: New York, 2007.
- (13) Petryayeva, E.; Krull, U. J. Localized Surface Plasmon Resonance: Nanostructures, Bioassays and Biosensing—A Review. *Anal. Chim. Acta* **2011**, *706*, 8–24.
- (14) Xu, H. X.; Aizpurua, J.; Kall, M.; Apell, P. Electromagnetic Contributions to Single-Molecule Sensitivity in Surface-Enhanced Raman Scattering. *Phys. Rev. E* **2000**, *62*, 4318–4324.
- (15) Muhlschlegel, P.; Eisler, H. J.; Martin, O. J. F.; Hecht, B.; Pohl, D. W. Resonant Optical Antennas. *Science* **2005**, *308*, 1607–1609.
- (16) Kinkhabwala, A.; Yu, Z. F.; Fan, S. H.; Avlasevich, Y.; Mullen, K.; Moerner, W. E. Large Single-Molecule Fluorescence Enhancements Produced by a Bowtie Nanoantenna. *Nat. Photonics* **2009**, *3*, 654–657.
- (17) Biagioni, P.; Huang, J. S.; Hecht, B. Nanoantennas For Visible and Infrared Radiation. *Rep. Prog. Phys.* **2012**, *75*, 1–40.
- (18) Kuhn, S.; Hakanson, U.; Rogobete, L.; Sandoghdar, V. Enhancement in Single-Molecule Fluorescence Using a Gold Nanoparticle as an Optical Nanoantenna. *Phys. Rev. Lett.* **2006**, *97*, 017402–1–017402–4.
- (19) Ming, T.; Chen, H. J.; Jiang, R. B.; Li, Q.; Wang, J. F. Plasmon-Controlled Fluorescence: Beyond the Intensity Enhancement. *J. Phys. Chem. Lett.* **2012**, *3*, 191–202.
- (20) Schuller, J. A.; Barnard, E. S.; Cai, W. S.; Jun, Y. C.; White, J. S.; Brongersma, M. L. Plasmonics For Extreme Light Concentration and Manipulation. *Nat. Mater.* **2010**, *9*, 193–204.
- (21) Kneipp, K.; Wang, Y.; Kneipp, H.; Perelman, L. T.; Itzkan, I.; Dasari, R.; Feld, M. S. Single Molecule Detection Using Surface-Enhanced Raman Scattering (SERS). *Phys. Rev. Lett.* **1997**, *78*, 1667–1670.

- (22) Nie, S. M.; Emery, S. R. Probing Single Molecules and Single Nanoparticles by Surface-Enhanced Raman Scattering. *Science* **1997**, *275*, 1102–1106.
- (23) Hirsch, L. R.; Stafford, R. J.; Bankson, J. A.; Sershen, S. R.; Rivera, B.; Price, R. E.; Hazle, J. D.; Halas, N. J.; West, J. L. Nanoshell-Mediated Near-Infrared Thermal Therapy of Tumors Under Magnetic Resonance Guidance. *Proc. Natl. Acad. Sci. U.S.A.* **2003**, *100*, 13549–13554.
- (24) Atwater, H. A.; Polman, A. Plasmonics for Improved Photovoltaic Devices. *Nat. Mater.* **2010**, *9*, 205–213.
- (25) Alu, A.; Engheta, N. Achieving Transparency With Plasmonic and Metamaterial Coatings. *Phys. Rev. E* **2005**, *72*, 016623/1–016623/9.
- (26) Cho, C.-H.; Asperti, C. O.; Turk, M. E.; Kikkawa, J. M.; Nam, S.-W.; Agarwal, R. Tailoring Hot-Exciton Emission and Lifetimes in Semiconducting Nanowires via Whispering-Gallery Nanocavity Plasmons. *Nat. Mater.* **2011**, *10*, 669–675.
- (27) Cho, C.-H.; Asperti, C. O.; Park, J.; Agarwal, R. Silicon Coupled with Plasmon Nanocavities Generates Bright Visible Hot Luminescence. *Nat. Photonics* **2013**, *7*, 285–289.
- (28) Akimov, A. V.; Mukherjee, A.; Yu, C. L.; Chang, D. E.; Zibrov, A. S.; Hemmer, P. R.; Park, H.; Lukin, M. D. Generation of Single Optical Plasmons in Metallic Nanowires Coupled to Quantum Dots. *Nature* **2007**, *450*, 402–406.
- (29) Oulton, R. F.; Sorger, V. J.; Zentgraf, T.; Ma, R.-M.; Gladden, C.; Dai, L.; Bartal, G.; Zhang, X. Plasmon Lasers at Deep Subwavelength Scale. *Nature* **2009**, *461*, 629–632.
- (30) Krasavin, A. V.; Zheludev, N. I. Active Plasmonics: Controlling Signals in Au/Ga Waveguide Using Nanoscale Structural Transformations. *Appl. Phys. Lett.* **2004**, *84*, 1416–1418.
- (31) Drexhage, K. H.; K, H.; Schäfer, F. P. Variation of the Fluorescence Decay Time of a Molecule in Front of a Mirror. *Ber. Bunsen-Ges. Phys. Chem.* **1968**, *72*, 329.
- (32) Siiman, O.; Lepp, A. Protonation of the Methyl-Orange Derivative of Aspartate Adsorbed on Colloidal Silver — A Surface-Enhanced Resonance Raman-Scattering and Fluorescence Emission Study. *J. Phys. Chem.* **1984**, *88*, 2641–2650.
- (33) Rubim, J. C.; Gutz, G. R.; Sala, O. Surface-Enhanced Raman-Scattering (SERS) and Fluorescence-Spectra from Mixed Copper(I)/Pyridine Iodide Complexes on a Copper Electrode. *Chem. Phys. Lett.* **1984**, *111*, 117–122.
- (34) Pockrand, I.; Brillante, A.; Möbius, D. Nonradiative Decay of Excited Molecules near a Metal-Surface. *Chem. Phys. Lett.* **1980**, *69*, 499–504.
- (35) Eagen, C. F.; Weber, W. H.; McCarthy, S. L.; Terhune, R. W. Time-Dependent Decay of Surface-Plasmon-Coupled Molecular Fluorescence. *Chem. Phys. Lett.* **1980**, *75*, 274–277.
- (36) Anger, P.; Bharadwaj, P.; Novotny, L. Enhancement and Quenching of Single-Molecule Fluorescence. *Phys. Rev. Lett.* **2006**, *96*, 113002/1–113002/4.
- (37) Biteen, J. S.; Pacifici, D.; Lewis, N. S.; Atwater, H. A. Enhanced Radiative Emission Rate and Quantum Efficiency in Coupled Silicon Nanocrystal–Nanostructured Gold Emitters. *Nano Lett.* **2005**, *5*, 1768–1773.
- (38) Chen, Y.; Munechika, K.; Ginger, D. S. Dependence of Fluorescence Intensity on the Spectral Overlap Between Fluorophores and Plasmon Resonant Single Silver Nanoparticles. *Nano Lett.* **2007**, *7*, 690–696.
- (39) Muskens, O. L.; Giannini, V.; Sanchez-Gil, J. A.; Rivas, J. G. Strong Enhancement of the Radiative Decay Rate of Emitters by Single Plasmonic Nanoantennas. *Nano Lett.* **2007**, *7*, 2871–2875.
- (40) Bakker, R. M.; Yuan, H. K.; Liu, Z. T.; Drachev, V. P.; Kildishev, A. V.; Shalaev, V. M.; Pedersen, R. H.; Gresillon, S.; Boltasseva, A. Enhanced Localized Fluorescence in Plasmonic Nanoantennae. *Appl. Phys. Lett.* **2008**, *92*, 043101/1.
- (41) Noginov, M. A.; Zhu, G.; Belgrave, A. M.; Bakker, R.; Shalaev, V. M.; Narimanov, E. E.; Stout, S.; Herz, E.; Suteewong, T.; Wiesner, U. Demonstration of a Spaser-Based Nanolaser. *Nature* **2009**, *460*, 1110–1113.
- (42) Dong, Z. C.; Zhang, X. L.; Gao, H. Y.; Luo, Y.; Zhang, C.; Chen, L. G.; Zhang, R.; Tao, X.; Zhang, Y.; Yang, J. L.; et al. Generation of Molecular Hot Electroluminescence by Resonant Nanocavity Plasmons. *Nat. Photonics* **2010**, *4*, 50–54.
- (43) Hofmann, C. E.; de Abajo, F. J. G.; Atwater, H. A. Enhancing the Radiative Rate in III–V Semiconductor Plasmonic Core–Shell Nanowire Resonators. *Nano Lett.* **2011**, *11*, 372–376.
- (44) Neogi, A.; Lee, C.-W.; Everitt, H. O.; Kuroda, T.; Tackeuchi, A.; Yablonovitch, E. Enhancement of Spontaneous Recombination Rate in a Quantum Well by Resonant Surface Plasmon Coupling. *Phys. Rev. B* **2002**, *66*, 153305/1–153305/4.
- (45) Okamoto, K.; Niki, I.; Shvartser, A.; Narukawa, Y.; Mukai, T.; Scherer, A. Surface-Plasmon-Enhanced Light Emitters Based on InGaN Quantum Wells. *Nat. Mater.* **2004**, *3*, 601–605.
- (46) Song, J.-H.; Atay, T.; Shi, S.; Urabe, H.; Nurmiikko, A. V. Large Enhancement of Fluorescence Efficiency from CdSe/ZnS Quantum Dots Induced by Resonant Coupling to Spatially Controlled Surface Plasmons. *Nano Lett.* **2005**, *5*, 1557–1561.
- (47) Okamoto, K.; Niki, I.; Scherer, A.; Narukawa, Y.; Mukai, T.; Kawakami, Y. Surface Plasmon Enhanced Spontaneous Emission Rate of InGaN/GaN Quantum Wells Probed by Time-Resolved Photoluminescence Spectroscopy. *Appl. Phys. Lett.* **2005**, *87*, 071102/1–071102/3.
- (48) Jun, Y. C.; Kekatpure, R. D.; White, J. S.; Brongersma, M. L. Nonresonant Enhancement of Spontaneous Emission in Metal–Dielectric–Metal Plasmon Waveguide Structures. *Phys. Rev. B* **2008**, *78*, 153111/1–153111/4.
- (49) Ma, R.-M.; Oulton, R. F.; Sorger, V. J.; Bartal, G.; Zhang, X. Room-Temperature Sub-Diffraction-Limited Plasmon Laser by Total Internal Reflection. *Nat. Mater.* **2011**, *10*, 110–113.
- (50) Bergman, D. J.; Stockman, M. I. Surface Plasmon Amplification by Stimulated Emission of Radiation: Quantum Generation of Coherent Surface Plasmons in Nanosystems. *Phys. Rev. Lett.* **2003**, *90*, 027402/1–027402/4.
- (51) Oulton, R. Surface Plasmon Lasers: Sources of Nanoscopic Light. *Mater. Today* **2012**, *15*, 26–34.
- (52) Pockrand, I.; Swalen, J. D.; Gordon, J. G.; Philpott, M. R. Exciton–Surface Plasmon Interactions. *J. Chem. Phys.* **1979**, *70*, 3401–3408.
- (53) Bellessa, J.; Bonnand, C.; Plenet, J. C.; Mugnier, J. Strong Coupling Between Surface Plasmons and Excitons in an Organic Semiconductor. *Phys. Rev. Lett.* **2004**, *93*, 036404/1–036404/4.
- (54) Bellessa, J.; Symonds, C.; Meynaud, C.; Plenet, J. C.; Cambril, E.; Miard, A.; Ferlazzo, L.; Lemaitre, A. Exciton/Plasmon Polaritons in GaAs/Al(0.93)Ga(0.07)As Heterostructures Near a Metallic Layer. *Phys. Rev. B* **2008**, *78*, 205326/1–205326/4.
- (55) Bellessa, J.; Symonds, C.; Vynck, K.; Lemaitre, A.; Brioude, A.; Beaur, L.; Plenet, J. C.; Viste, P.; Felbacq, D.; Cambril, E.; et al. Giant Rabi Splitting Between Localized Mixed Plasmon–Exciton States in a Two-Dimensional Array of Nanosize Metallic Disks in an Organic Semiconductor. *Phys. Rev. B* **2009**, *80*, 033303/1–033303/4.
- (56) Gomez, D. E.; Vernon, K. C.; Mulvaney, P.; Davis, T. J. Surface Plasmon Mediated Strong Exciton–Photon Coupling in Semiconductor Nanocrystals. *Nano Lett.* **2010**, *10*, 274–278.
- (57) Achermann, M. Exciton–Plasmon Interactions in Metal–Semiconductor Nanostructures. *J. Phys. Chem. Lett.* **2010**, *1*, 2837–2843.
- (58) Yang, P. D.; Yan, R. X.; Fardy, M. Semiconductor Nanowire: What's Next? *Nano Lett.* **2010**, *10*, 1529–1536.
- (59) Li, Y.; Qian, F.; Xiang, J.; Lieber, C. M. Nanowire Electronic and Optoelectronic Devices. *Mater. Today* **2006**, *9*, 18–27.
- (60) Agarwal, R.; Lieber, C. M. Semiconductor Nanowires: Optics and Optoelectronics. *Appl. Phys. A* **2006**, *85*, 209–215.
- (61) Agarwal, R. Heterointerfaces in Semiconductor Nanowires. *Small* **2008**, *4*, 1872–1893.
- (62) Nobis, T.; Kaidashev, E. M.; Rahm, A.; Lorenz, M.; Grundmann, M. Whispering Gallery Modes in Nanosized Dielectric Resonators with Hexagonal Cross Section. *Phys. Rev. Lett.* **2004**, *93*, 103903/1–103903/4.

- (63) Cao, L. Y.; White, J. S.; Park, J. S.; Schuller, J. A.; Clemens, B. M.; Brongersma, M. L. Engineering Light Absorption in Semiconductor Nanowire Devices. *Nat. Mater.* **2009**, *8*, 643–647.
- (64) Snyder, W.; J. D. L *Optical Waveguide Theory*; Chapman and Hall: London, 1983.
- (65) van Vugt, L. K.; Zhang, B.; Piccione, B.; Spector, A. A.; Agarwal, R. Size-Dependent Waveguide Dispersion in Nanowire Optical Cavities: Slowed Light and Dispersionless Guiding. *Nano Lett.* **2009**, *9*, 1684–1688.
- (66) Hayden, O.; Agarwal, R.; Lieber, C. M. Nanoscale Avalanche Photodiodes for Highly Sensitive and Spatially Resolved Photon Detection. *Nat. Mater.* **2006**, *5*, 352–356.
- (67) Sirbuli, D. J.; Tao, A.; Law, M.; Fan, R.; Yang, P. Multifunctional Nanowire Evanescent Wave Optical Sensors. *Adv. Mater.* **2007**, *19*, 61–66.
- (68) Coleman, J. J.; Bryce, A. C.; Jagadish, C. *Advances in Semiconductor Lasers*, 1st ed.; Elsevier/Academic Press: Amsterdam, The Netherlands; Boston, MA, 2012; Vol. XIV, p 526.
- (69) Ma, Y. G.; Guo, X.; Wu, X. Q.; Dai, L.; Tong, L. M. Semiconductor Nanowire Lasers. *Adv. Opt. Photonics* **2013**, *5*, 216–273.
- (70) Law, M.; Greene, L. E.; Johnson, J. C.; Saykally, R.; Yang, P. D. Nanowire Dye-Sensitized Solar Cells. *Nat. Mater.* **2005**, *4*, 455–459.
- (71) Cao, L. Y.; Fan, P. Y.; Vasudev, A. P.; White, J. S.; Yu, Z. F.; Cai, W. S.; Schuller, J. A.; Fan, S. H.; Brongersma, M. L. Semiconductor Nanowire Optical Antenna Solar Absorbers. *Nano Lett.* **2010**, *10*, 439–445.
- (72) Oraevsky, A. N. Whispering-Gallery Waves. *Quantum Electron.* **2002**, *32*, 377–400.
- (73) Matsko, A. B.; Ilchenko, V. S. Optical Resonators with Whispering-Gallery Modes — Part I: Basics. *IEEE J. Sel. Top. Quantum Electron.* **2006**, *12*, 3–14.
- (74) Piccione, B.; Agarwal, R.; Jung, Y.; Agarwal, R. Size-Dependent Chemical Transformation, Structural Phase Change, and Optical Properties of Nanowires. *Philos. Mag.* **2013**, *93*, 2089–2121.
- (75) Piccione, B.; Aspetti, C. O.; Cho, C.-H.; Agarwal, R. Tailoring Light-Matter Coupling in Semiconductor and Hybrid-Plasmonic Nanowires. *Rep. Prog. Phys.* **2014**, *77*, 1–20.
- (76) van Vugt, L. K.; Piccione, B.; Cho, C.-H.; Nukala, P.; Agarwal, R. One-Dimensional Polaritons with Size-Tunable and Enhanced Coupling Strengths in Semiconductor Nanowires. *Proc. Natl. Acad. Sci. U.S.A.* **2011**, *108*, 10050–10055.
- (77) Piccione, B.; Cho, C. H.; van Vugt, L. K.; Agarwal, R. All-Optical Active Switching in Individual Semiconductor Nanowires. *Nat. Nanotechnol.* **2012**, *7*, 640–645.
- (78) Mertens, H.; Koenderink, A. F.; Polman, A. Plasmon-Enhanced Luminescence Near Noble-Metal Nanospheres: Comparison of Exact Theory and an Improved Gersten and Nitzan Model. *Phys. Rev. B* **2007**, *76*, 115123/1–115123/12.
- (79) Barnes, W. L. Fluorescence Near Interfaces: The Role of Photonic Mode Density. *J. Mod. Opt.* **1998**, *45*, 661–699.
- (80) Oulton, R. F.; Sorger, V. J.; Genov, D. A.; Pile, D. F. P.; Zhang, X. A Hybrid Plasmonic Waveguide for Subwavelength Confinement and Long-Range Propagation. *Nat. Photonics* **2008**, *2*, 496–500.
- (81) Wiesner, P.; Heim, U. Dynamics of Exciton–Polariton Recombination in CdS. *Phys. Rev. B* **1975**, *11*, 3071–3077.
- (82) Dassarma, S.; Jain, J. K.; Jalabert, R. Hot-Electron Relaxation in GaAs Quantum Wells. *Phys. Rev. B* **1988**, *37*, 1228–1230.
- (83) Kasha, M. Characterization of Electronic Transitions in Complex Molecules. *Discuss. Faraday Soc.* **1950**, *9*, 14–19.
- (84) van Vugt, L. K.; Piccione, B.; Cho, C. H.; Aspetti, C.; Wirshba, A. D.; Agarwal, R. Variable Temperature Spectroscopy of As-Grown and Passivated CdS Nanowire Optical Waveguide Cavities. *J. Phys. Chem. A* **2011**, *115*, 3827–3833.
- (85) Thomas, D. G.; Hopfield, J. J. Exciton Spectrum of Cadmium Sulfide. *Phys. Rev.* **1959**, *116*, 573–582.
- (86) Gross, E.; Permogor, S.; Travnikov, V.; Selkin, A. Hot Excitons and Exciton Excitation Spectra. *J. Phys. Chem. Solids* **1970**, *31*, 2595–2606.
- (87) Kippenberg, T. J.; Kalkman, J.; Polman, A.; Vahala, K. J. Demonstration of an Erbium-Doped Microdisk Laser on a Silicon Chip. *Phys. Rev. A* **2006**, *74*, 051802/1–051802/4.
- (88) Zhang, J.; Li, D. H.; Chen, R. J.; Xiong, Q. H. Laser Cooling of a Semiconductor by 40 K. *Nature* **2013**, *493*, 504–508.
- (89) Pavesi, L.; Lockwood, D. J. Alumni and Friends Memorial Book Fund. *Silicon Photonics*. Springer: Berlin, Germany; New York, 2004; Vol. XVI, p 397.
- (90) Goldman, J. R.; Prybyla, J. A. Ultrafast Dynamics of Laser-Excited Electron Distributions in Silicon. *Phys. Rev. Lett.* **1994**, *72*, 1364–1367.
- (91) Sabbah, A. J.; Riffe, D. M. Femtosecond Pump–Probe Reflectivity Study Of Silicon Carrier Dynamics. *Phys. Rev. B* **2002**, *66*, 165217/1–165217/11.
- (92) de Boer, W. D. A. M.; Timmerman, D.; Dohnalova, K.; Yassievich, I. N.; Zhang, H.; Buma, W. J.; Gregorkiewicz, T. Red Spectral Shift and Enhanced Quantum Efficiency in Phonon-Free Photoluminescence from Silicon Nanocrystals. *Nat. Nanotechnol.* **2010**, *5*, 878–884.
- (93) Yu, P. Y.; Cardona, M. *Fundamentals of Semiconductors: Physics and Materials Properties*, 3rd ed.; Springer: Berlin, Germany; New York, 2001.
- (94) Liang, D.; Bowers, J. E. Recent Progress in Lasers on Silicon. *Nat. Photonics* **2010**, *4*, 511–517.
- (95) Khitrova, G.; Gibbs, H. M.; Kira, M.; Koch, S. W.; Scherer, A. Vacuum Rabi Splitting in Semiconductors. *Nat. Phys.* **2006**, *2*, 81–90.
- (96) Permogorov, S. Hot Excitons in Semiconductors. *Phys. Status Solidi B* **1975**, *68*, 9–42.
- (97) Aspetti, C. O.; Cho, C.-H.; Agarwal, R.; Agarwal, R. Studies of Hot Photoluminescence in Plasmonically Coupled Silicon via Variable Energy Excitation and Temperature-Dependent Spectroscopy. *Nano Lett.* **2014**, *14*, 5413–5422.
- (98) Kwack, H. S.; Sun, Y.; Cho, Y. H.; Park, N. M.; Park, S. J. Anomalous Temperature Dependence of Optical Emission in Visible-Light-Emitting Amorphous Silicon Quantum Dots. *Appl. Phys. Lett.* **2003**, *83*, 2901–2903.
- (99) Jiang, D. S.; Jung, H.; Ploog, K. Temperature-Dependence of Photoluminescence from GaAs Single and Multiple Quantum-Well Heterostructures Grown by Molecular-Beam Epitaxy. *J. Appl. Phys.* **1988**, *64*, 1371–1377.
- (100) Venkateswarlu, K. Temperature Dependence of the Intensities of Raman Lines. *Nature* **1947**, *159*, 96–97.
- (101) Compaan, A.; Trodahl, H. J. Resonance Raman-Scattering in Si at Elevated-Temperatures. *Phys. Rev. B* **1984**, *29*, 793–801.
- (102) Hyun, J. K.; Lauhon, L. J. Spatially Resolved Plasmonically Enhanced Photocurrent from Au Nanoparticles on a Si Nanowire. *Nano Lett.* **2011**, *11*, 2731–2734.
- (103) Wang, J.; Gudiksen, M. S.; Duan, X.; Cui, Y.; Lieber, C. M. Highly Polarized Photoluminescence and Photodetection from Single Indium Phosphide Nanowires. *Science* **2001**, *293*, 1455–1457.
- (104) Xiang, J.; Lu, W.; Hu, Y.; Wu, Y.; Yan, H.; Lieber, C. M. Ge/Si Nanowire Heterostructures as High-Performance Field-Effect Transistors. *Nature* **2006**, *441*, 489–493.
- (105) Yan, H.; Choe, H. S.; Nam, S. W.; Hu, Y. J.; Das, S.; Klemic, J. F.; Ellenbogen, J. C.; Lieber, C. M. Programmable Nanowire Circuits for Nanoprocessors. *Nature* **2011**, *470*, 240–244.
- (106) Oldenburg, S. J.; Averitt, R. D.; Westcott, S. L.; Halas, N. J. Nanoengineering of Optical Resonances. *Chem. Phys. Lett.* **1998**, *288*, 243–247.
- (107) Yu, K.; Lakhani, A.; Wu, M. C. Subwavelength Metal–Optic Semiconductor Nanopatch Lasers. *Opt. Express* **2010**, *18*, 8790–8799.
- (108) Nezhad, M. P.; Simic, A.; Bondarenko, O.; Slutsky, B.; Mizrahi, A.; Feng, L. A.; Lomakin, V.; Fainman, Y. Room-Temperature Subwavelength Metallo-Dielectric Lasers. *Nat. Photonics* **2010**, *4*, 395–399.
- (109) Ni, C. Y. A.; Chang, S. W.; Gargas, D. J.; Moore, M. C.; Yang, P. D.; Chuang, S. L. Metal-Coated Zinc Oxide Nanocavities. *IEEE J. Quantum Electron.* **2011**, *47*, 245–251.